Copper-Basic Sites Synergic Effect on the Ethanol Dehydrogenation and Condensation Reactions

Jorge Quesada,[a] Laura Faba,[a] Eva Díaz,[a] and Salvador Ordóñez*[a]

Bioethanol upgrading through condensation is of key interest in the development of sustainable processes, shifting from fossil to renewable carbon. Here, a new strategy is proposed, which combines in one catalyst an appropriate distribution of acid/basic sites of a mixed oxide with the presence of an active dehydrogenation phase (Cu nanoparticles). Experiments, performed in a fixed bed reactor, reveal a very positive effect of Cu in the performance of Mg–Al catalyst, with 1-butanol productivity 12 times higher at 523 K under inert conditions. The improvement is even more notable in presence of H_2, almost 30 times higher, under same conditions. The presence of Cu on the surface increases the formation of acetaldehyde, limiting the extent of dehydration side-reactions. In addition, hydrogen enhances the C4 hydrogenation, preventing oligomerizations and inhibiting decarbonylation steps that are directly related to the catalytic deactivation by poisoning.

Introduction

The dehydrogenation of alcohols to aldehydes and ketones is one of the most important steps in the field of the production of added-value chemicals from alcohols.[1] Concerning primary alcohols (R–CH_2–OH) and heterogeneous catalysis, the corresponding aldehydes obtained by dehydrogenation interact with the catalytic surface, resulting in the formation of intermediate moieties, such as enolates (R–CH*–CH=O) and acyls (R–CH_2–C*=O*). These surface intermediates are energetically stabilized by acid-basic pair sites or metal nanoparticles.[2,3] Subsequently, these species can undergo the formation of C–C and C–O bonds by aldol condensation and esterification reactions, respectively, leading to larger oxygenates with higher value as chemical precursors.[3,4] Consequently, catalytic dehydrogenation has a high upgrading potential for biomass-derived compounds, such as ethanol.

Ethanol upgrading is accomplished via different reactions,[5] being the Guerbet reaction one of the most widely proposed.[6] This reaction enables to obtain higher alcohols, 1-butanol in this case, from two shorter alcohols (ethanol) via aldol condensation.[7] Essentially, the Guerbet reaction consists of four steps (alcohol dehydrogenation to corresponding aldehyde, aldolization of the aldehyde followed by dehydration of the formed aldol, and two hydrogenations of the respective α,β-unsaturated aldehyde yielded in the previous step) shown in Scheme 1.[7,8] According to this complex mechanisms, there is not agreement about the key step of the process. Several authors highlight the aldolization step (C–C bond formation) as the key step, focusing the efforts on in the development of active catalysts with acid/basic pairs.[8,9] By contrast, other researchers suggest that the whole process is conditioned by the first abstraction of the αH, because of the higher activation energy barrier of this step in comparison to the aldolization one, requiring higher temperatures to take place.[7] Considering both perspectives, modifying the acid-base catalysts (such as basic mixed oxides) by supporting metal nanoparticles (with demonstrated dehydrogenation activity) on their surface would allow improving this first step and, as a consequence, the

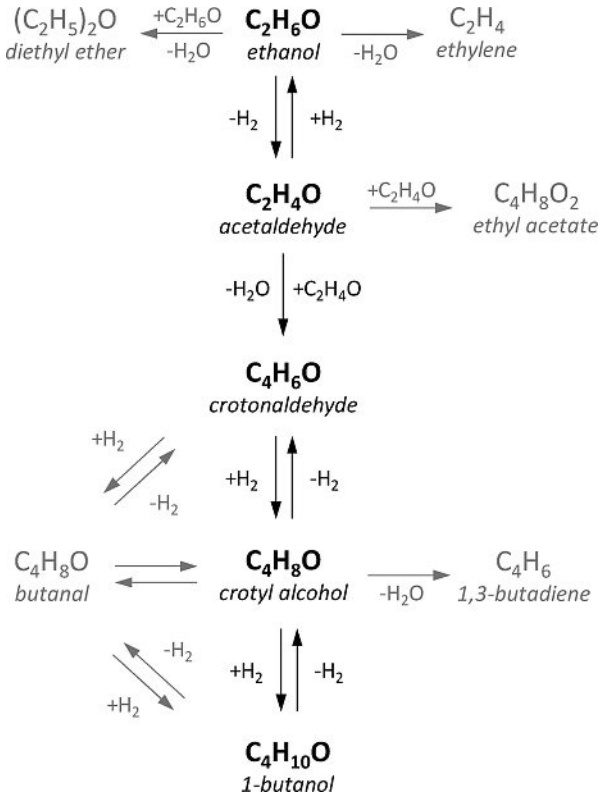

Scheme 1. Proposed reaction mechanism in the ethanol condensation.[7,8] The Guerbet reaction is the main pathway (indicated in black and bold); side reactions are depicted in grey.

[a] *J. Quesada, Dr. L. Faba, Dr. E. Díaz, Prof. S. Ordóñez*
Department of Chemical and Environmental Engineering
University of Oviedo
Av. Julián Clavería s/n, Oviedo, 33006 (Spain)
E-mail: sordonez@uniovi.es

Supporting information for this article is available on the WWW under https://doi.org/10.1002/cctc.201800517

performance of the whole process. Copper has been reported as the most selective metal promoting alcohol dehydrogenation.[10] In recent works,[11–13] some authors used copper supported on metal oxides (CeO_2 and ZrO_2) in the ethanol upgrading with the aim of improving the 1-butanol or ethyl acetate productionm obtaining satisfactory results. Nevertheless, the copper loadings ($\geq$5 wt.%) were fairly high,[11–13] masking the effect of the acid and basic site of the oxide. There are also works concerning this reaction in which other transition metals (e.g., iron, nickel, cobalt) were supported on different oxides (CeO_2 and MgAlO), but, again, with a relative high metal content (5–10 wt.%).[14]

The role of the addition of Cu nanoparticles on the performance of magnesia-alumina mixed oxides (Mg–Al) used as catalyst for the ethanol gas-phase Guerbet reaction to 1-butanol is studied in this paper. Mg–Al was chosen as support because of its well-known behavior for the ethanol condensation (allowing discerning the real effect of Cu nanoparticles),[15–17] as well as its reasonable good activity comparing other materials tested in this reaction.[18] Low metal loadings (1 wt.%) were used in order to minimize the blockage and modification of the original acid/basic sites distribution of the parent mixed oxide.

In order to get a better understanding of the role of this metal, results achieved with the Cu/Mg–Al material were compared with those reached with copper supported on an inert material (Cu/SiO_2) and a physical mixture of Cu/SiO_2 and Mg–Al mixed oxide. Gas chromatography and *in situ* infrared spectroscopic (Diffuse Reflectance Infrared Fourier Transform Spectroscopy, DRIFTS) techniques were used for analyzing the different compounds yielded during the reaction, as well as their interaction with the catalyst surface.

Results and Discussion

Experiments were selected in order to have a better understanding of the synergic effect of copper and acid-basic sites distribution of the parent basic mixed oxide, also considering the role of the copper nanoparticles in the hydrogen activation. Thus, three different catalysts were studied: parent Mg–Al mixed oxide, copper supported in this oxide, and a physical mixture of the oxide with Cu/SiO_2 catalyst (SiO_2 is considered to have negligible acid-base activity, as it is also demonstrated in the characterization section). All the catalysts were tested both, in presence and in absence of hydrogen. The maximum temperature considered was 723 K, in order to discard the copper nanoparticles sintering.

Figure 1 shows the 1-butanol productivity, under inert or reducing atmosphere, as function of the reaction temperature. In absence of hydrogen, the highest butanol production-rates were obtained with the bifunctional material (Cu/Mg–Al), being the differences more relevant at soft conditions. This rate reaches a maximum of 1600 $\mu mol\,ks^{-1}\,g^{-1}$ at 723 K. This value corresponds to a 37.1% of conversion and 25.0% butanol selectivity. If hydrogen is fed, results with Cu/Mg–Al are even better, observing improvements up to 150% when results at

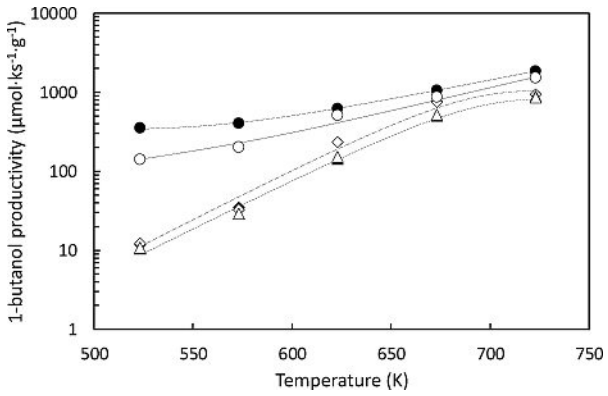

Figure 1. Evolution of the 1-butanol productivity with the temperature using Mg–Al* (♦); Cu/Mg–Al (●); Cu/SiO_2 + Mg–Al (▲). Black symbols correspond to reducing conditions (20 NmL min^{-1} 10 vol.% H_2/He); white symbols correspond to inert conditions (20 NmL h^{-1} of He). *Values under inert conditions are obtained from reference [17]. *Dashed lines are meant to guide the eye.*

523 K are compared. Considering that hydrogen obtained during dehydrogenation step is stoichiometrically enough to accomplish the hydrogenations, the different behavior observed under inert or reducing atmosphere suggests that hydrogen atoms released in the first step (ethanol dehydrogenation) are not efficiently used in the hydrogenation steps, recombining itself and desorbing as molecular hydrogen when working under inert atmosphere.

It can be presumed that results obtained with Cu/Mg–Al could be partially limited by the lack of acid/basic sites (supporting metals affects to the original distribution of acidity and basicity). Thus, the activity of a physical mixture of the two catalysts was considered (Mg-Al for the acid/basic sites, and Cu/SiO_2 for the dehydrogenation/hydrogenation steps). With this approach, the role of metal could be analyzed preventing any change in the original surface chemistry of the mixed oxide. Results are also considered in Figure 1. In this case, the productivity of 1-butanol was calculated taking into account only the mass of Mg–Al. This was considered in view of the results obtained when using Cu/SiO_2 for the reaction, as it is explained below.

Comparing the trends of Cu/Mg–Al and the physical mixture, it can be concluded that the expected improvement was not reached, obtained better results with Cu/Mg–Al, even in absence of hydrogen. This fact highlights the key role of the spatial proximity between the metal-phase and the acid-basic active sites. In the physical mixture, the hydrogen atoms produced during the dehydrogenation (on the Cu/SiO_2) cannot react with crotonaldehyde obtained on the Mg–Al (active sites in different phases), producing the recombination and desorption as inactive H_2. On the contrary, in the Cu/Mg–Al, the proximity between both active sites enhances the involvement of hydrogen atoms in those elementary steps leading to hydrogen-saturated molecules, such as butanol. This hypothesis is congruent with the well-known hydrogen spill-over that allows the mobility of hydrogen atoms on mixed oxides by a Grotthuss-type mechanism.[19] Using the physical mixture, as

there is not possible hydrogen spill-over, the Meerwein-Ponndorf-Verley (MPV) reduction is the main hydrogenation mechanism.[8] Because of this, the performance of the reaction, in terms of 1-butanol productivity, is the same under reducing or inert conditions. According to this assumption, the positive effect of reducing atmosphere on the behavior of the bifunctional material and the negligible effect of this parameter in the performance of the physical mixture are justified.

If the physical mixture is compared with the results of the parent Mg–Al, a very similar behavior was observed, with slight variations (highest difference observed at 623 K: 236 and 154 $\mu mol\,ks^{-1}\,g^{-1}$ with the Mg–Al and the physical mixture, respectively). In any case, all these values are significantly lower than those data obtained with the Cu/Mg–Al, mainly at low temperatures (lowest difference observed at 673 K, under inert conditions: 881 and 758 $\mu mol\,ks^{-1}\,g^{-1}$ with the Cu/Mg–Al and the Mg–Al, respectively).

The high dependence of the reaction temperature in the cases of the Mg–Al and the physical mixture (comparing with the bifunctional), and its stabilization at the highest temperatures, is explained by the different surface chemistry of these materials, mainly in terms of strength of the acid and basic sites. These results suggest that there is more than one active site involved in the reactions catalyzed by Mg–Al and the physical mixture, needing a minimum temperature to activate them, whereas in the case of the bifunctional catalyst, this effect does not take place, a linear evolution being observed.

In order to check this hypothesis, all the materials were characterized, analyzing the morphological properties as well as the surface chemistry. Main results are summarized in Table 1. Whereas the morphological properties are rather similar for both Mg–Al and Cu/Mg–Al, the distribution and concentration of the active sites reveal several differences. Concerning the acidity, most of the original acid sites are blocked by copper nanoparticles, being this effect more notable for the strongest ones. The concentration of these acid sites is much lower for the Cu/Mg–Al, hence the amount of Lewis acid and acid-basic pair sites, which promote the MPV reduction,[20] is significantly higher for the Mg-Al leading to higher ability of this material (or physical mixture) in performing this reaction. These sort of active sites are also related to non-desired dehydrations (obtaining ethylene and 1,3-butadiene). These dehydrations are more relevant over 650 K, justifying the flat profile observed at the last points. Regarding the concentration of weak and medium strength basic sites (sites required for the aldolization step[12]), it is similar with the two materials. On the other hand, the concentration of strong basic sites (as in the case of the acid ones) is much lower for the bifunctional catalyst, comparing with the parent Mg-Al. This entails less ability to promote dehydration reactions by none of the two elimination mechanisms (E_{1cB} and E_2, with the strong basic and acid, respectively).[15]

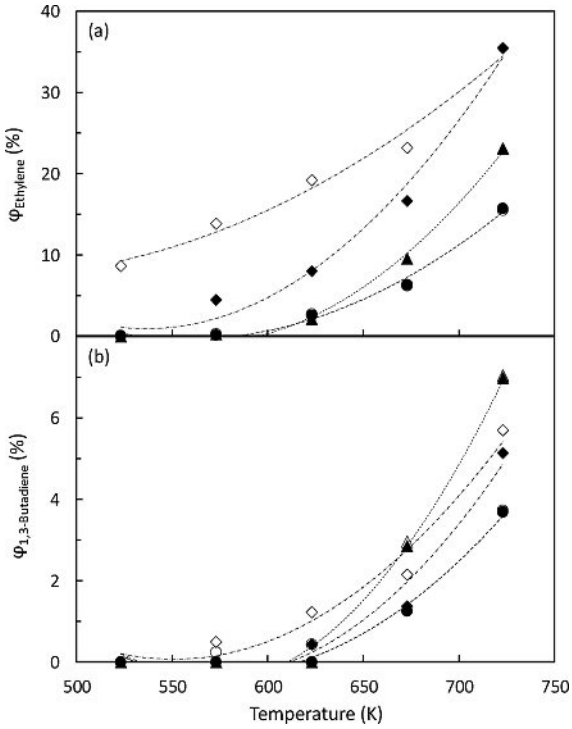

Figure 2. Selectivity evolution of the dehydration products: (a) ethylene and (b) 1,3-butadiene, with the temperature under reducing and inert conditions using: Mg–Al* (◆), Cu/Mg–Al (●), and Cu/SiO_2 + Mg–Al (▲). Black symbols: reducing conditions (20 NmL min^{-1} 10 vol.% H_2/He); white symbols: inert conditions (20 NmL h^{-1} of He). *Values under inert conditions are obtained from reference [17].

In order to determine the relevance of dehydration side-reactions, the ethylene and 1,3-butadiene selectivities are shown in Figure 2. Selectivities (φ) were calculated as it is explained in the Experimental Section. As it was expected, the selectivities to both compounds increase as temperature increases for all the catalysts, both in presence and in absence of hydrogen, being the effect of the temperature more relevant for the parent Mg–Al and the physical mixture, in good agreement with the previous discussion. As to the role of the hydrogen on the dehydration steps, its presence only affects the behavior of the Mg–Al catalyst, suggesting a competitive adsorption of molecular hydrogen on the strong acid sites

Table 1. Characterization results of the mixed oxides: Morphological properties, and density and distribution of the basic and acid sites. Temperatures in brackets corresponds to each maximum of the TPD profiles. *Values reported in a previous work.[17]

	Morphological properties			Basic sites [$\mu mol\,g^{-1}$], (T [K])			Acid sites [$\mu mol\,g^{-1}$], (T [K])		
	S_{BET} [$m^2\,g^{-1}$]	V_p [$cm^3\,g^{-1}$]	D_p [nm]	weak	medium	strong	weak	medium	strong
Mg–Al*	226	0.7	13.5	49.7, (340)	71.7, (400)	238.6, (630,670,800)	11.3, (345,370)	12.5, (450)	41.8, (630,800)
Cu/Mg–Al	206	0.5	5.6	62.5, (330,365)	73.1, (455)	62.5, (660,715)	4.4, (330,375)	2.1, (450)	3.1, (545)
Cu/SiO_2	160	1.2	27.3	–	–	–	–	–	–

related to OH groups. This hypothesis was previously reported catalyzing the H_2–D_2 equilibration on magnesia and alumina oxides.[21,22] Nevertheless, this effect is less significant, even negligible, at the highest temperatures, as the importance of these OH sites is lower at increasing temperatures.[22] For instance, with Mg–Al, under 600 K (conditions at which conversion of the different catalysts are more similar) there are significant differences in the selectivity to ethylene (Figure 2a; 13.8 and 4.5% under inert and reducing conditions, respectively). This effect, which could be also expected for the physical mixture, is not observed (same profile with and without H_2) because of the preferential adsorption of this molecule on Cu nanoparticles, masking the effect of OH sites of the Mg–Al. This negligible influence of hydrogen is also observed with the Cu/Mg–Al, in good agreement with the previous justification. In addition, the lower strong acid sites concentration justifies the low dehydration selectivities obtained with this material.

The competitive adsorption on the acid sites promoted by OH groups is also noticed analyzing the evolution of 1,3-butadiene, only observing effects due to the hydrogen presence for Mg-Al. However, in this case, the physical mixture seems to be more selective to this compound than the parent Mg-Al, in contrast to what is happening with ethylene. The analysis of these profiles is not so evident, considering that 1,3-butadiene is a C4 compound, being its selectivity not only conditioned by the corresponding active sites but also by the activity in the previous steps, required to obtain the acetaldehyde that promotes the aldol condensation.

The evolution of acetaldehyde selectivity with the reaction temperature is presented in Figure 3. The clear profile of a primary reaction product undergoing further reaction is observed, decreasing the selectivity with the temperature. The same behavior is observed with the three catalytic systems, suggesting that same mechanism (Guerbet reaction) prevails in all the cases. Despite the analyzed temperature, the highest acetaldehyde selectivity is obtained with the physical mixture (improvements up to 141.7% comparing the Mg–Al) because

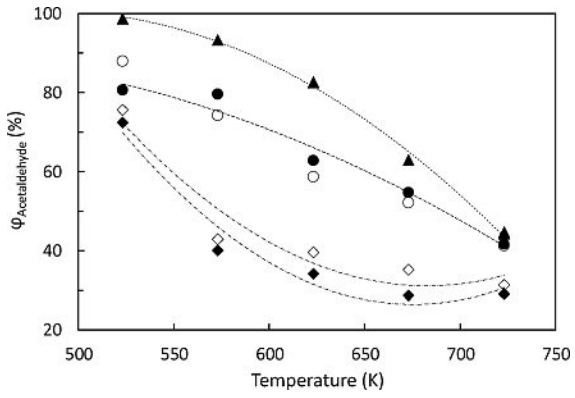

Figure 3. Acetaldehyde selectivity evolution with the temperature under reducing and inert conditions using: Mg–Al* (◆), Cu/Mg–Al (●), and Cu/SiO_2 + Mg–Al (▲). Black symbols: reducing conditions (20 NmL min^{-1} 10 vol.% H_2/He); white symbols: inert conditions (20 NmL h^{-1} of He). *Values under inert conditions are obtained from reference [17].

of the Cu/SiO_2 dehydrogenating functionality. Therefore, there is much more acetaldehyde in the reaction medium when working with the physical mixture, with same values under inert or reducing conditions. The formation of crotonaldehyde directly depends on the acetaldehyde available because of: (i) the aldolization is an acetaldehyde bimolecular non-equilibrated step,[8] and (ii) the concentration and distribution of the active sites that favors this step are the same with both materials. 1,3-butadiene is obtained from crotyl alcohol (as a side product after the first hydrogenation of crotonaldehyde), so the highest amount of acetaldehyde is directly related to the highest 1,3-butadiene selectivity observed for the physical mixture.

It must be also considered that crotyl alcohol is not only the precursor of 1,3-butadiene, but also of 1-butanol. For instance, the 1-butanol/1,3-butadiene selectivity ratio when working under reducing atmosphere is 4.3 at 673 K with the physical mixture, whereas it is 21.9 with the bare Mg–Al. This increase of the selectivity to 1,3-butadiene against 1-butanol when using the physical mixture might be related to a lower amount of hydrogen adatoms on the surface of the acid-basic component of the mixture (Mg–Al) where the unsaturated intermediates are adsorbed. This idea would be justified considering that an important part of the acetaldehyde molecules generated on the Cu/SiO_2 particles are desorbed to the reaction medium and then adsorbed on the Mg–Al component, where the aldol condensation is carried out. Consequently, the quantity of hydrogen adatoms on the Mg–Al is lower with the physical mixture inasmuch as significant part of the ethanol dehydrogenation is not performed on the Mg–Al component. Thus, although the reduction of the crotonaldehyde to crotyl alcohol can be accomplished by the MPV reaction, the hydrogenation ability of the C=C bond of the crotyl alcohol to form 1-butanol (performed by hydrogen adatoms) is lower than that observed with the parent Mg–Al.

Considering that hydrogenations are the last steps, they are conditioned by the activity in the previous ones, and a deeper analysis of this stage requires relative analyses considering the compounds involved by lumped families. Thus, the analysis of the evolution of the selectivity ratio between the sum of all the compounds obtained from crotonaldehyde hydrogenation and further reactions (C4 hydrogenated: crotyl alcohol, butanal, 1,3-butadiene, and 1-butanol) and the sum of the compounds formed from the aldolization step (C4 aldolization: crotonaldehyde + C4 hydrogenated) is depicted in Figure 4. This figure shows that the hydrogenation ability of the physical mixture is lower than that achieved with the parent Mg–Al. Furthermore, it confirms that the presence of molecular hydrogen does not have any effect on the hydrogenation, except when working with the bifunctional catalyst.

The difference in dehydrogenation and hydrogenation capabilities of these catalytic-systems is much clearly observed when the same selectivity ratio is plotted versus the acetaldehyde selectivity, as it is observed in Figure 5. Whereas values corresponding to the bare Mg–Al demonstrate higher hydrogenation ability with regard to dehydrogenation, the physical mixture exhibits the opposite behavior. By contrast,

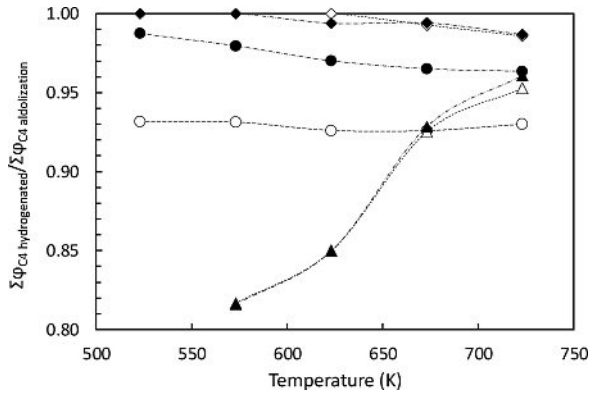

Figure 4. Analysis of the evolution of the hydrogenated C4-aldolization C4 selectivity ratio with the temperature under presence and absence of hydrogen using: Mg–Al* (◆), Cu/Mg–Al (●), and Cu/SiO_2 + Mg–Al (▲). Black symbols: reducing conditions (20 NmL min^{-1} 10 vol.% H_2/He); white symbols: inert conditions (20 NmL h^{-1} of He). *Values under inert conditions are obtained from reference [17].

the bifunctional system seems to gather both functionalities, especially in presence of molecular hydrogen, combining large acetaldehyde selectivities with high hydrogenation activities.

Another enhancement directly related to the prevalence of hydrogenation steps is the hindrance of undesired oligomerization processes. In order to check this hypothesis, the evolution of carbon balance closure is plotted in Figure 6a. Carbon balance closure is over 75 % with the three materials at all the considered temperatures. In general, higher conversion (Figure 6b) implies lower carbon balance closure, because non-identified compounds (oligomers, not considered for the calculations) tend to be formed. At this point, it must be highlighted that all the compounds depicted in the Scheme 1 are perfectly quantified, being the yields of the minor ones included in the Supporting Information (Table S1). Comparing among the three catalysts, carbon balances are higher for the Cu/Mg–Al especially at low temperatures, despite being the

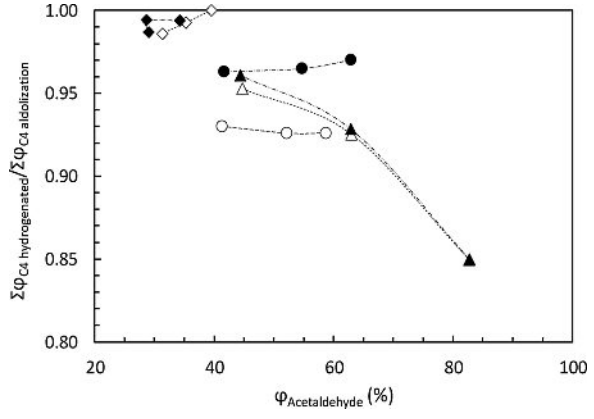

Figure 5. Analysis of the evolution of the hydrogenated C4-aldolization C4 selectivity ratio versus the acetaldehyde selectivity under presence or absence of hydrogen using: Mg-Al* (◆), Cu/Mg-Al (●), and Cu/SiO_2 + Mg-Al (▲). Black symbols: reducing conditions (20 NmL min^{-1} 10 vol.% H_2/He); white symbols: inert conditions (NmL·h^{-1} of He). *Values under inert conditions are obtained from reference [17].

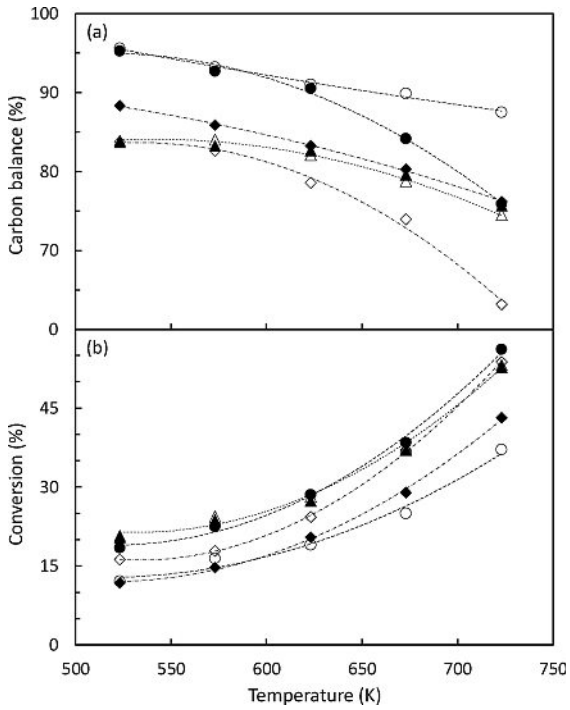

Figure 6. Evolution of: (a) carbon balance closure and (b) conversion, with the temperature under reducing and inert conditions using: Mg–Al* (◆), Cu/Mg–Al (●), and Cu/SiO_2 + Mg–Al (▲). Black symbols: reducing conditions (20 NmL min^{-1} 10 vol.% H_2/He); white symbols: inert conditions (20 NmL h^{-1} of He). *Values under inert conditions are obtained from reference [17].

conversion lower with the other two materials. This is due to the much higher selectivity towards the main route (1-butanol yield) observed when using the bifunctional material. Regarding the Mg–Al and the physical mixture, conversions are lower with the Mg–Al mainly at mild conditions (11.8 and 20.5 % at 523 K with the Mg–Al and the physical mixture, respectively, under reducing conditions) because of the enhancement of the ethanol dehydrogenation with the physical mixture due to the copper presence.

In order to stress the role of copper in the ethanol gas-phase condensation, experiments were carried out using only the Cu/SiO_2 material and comparing the data obtained with the previous results with the bifunctional one. This analysis is only possible if copper crystallite size distribution is similar, since this parameter significantly affects its behavior in these reaction systems.[2] Figure 7 shows the particle size distribution and TPR results of both Cu/Mg-Al and Cu/SiO_2 (HRTEM representative micrographs are included in the Supporting Information, Figure S1). Taking into account that similar copper particle sizes were obtained with both materials (1.4 and 1.9 nm for the Cu/Mg–Al and Cu/SiO_2, respectively), the conclusions drawn from the functionality of copper when using Cu/SiO_2 can be extrapolated to the Cu/Mg–Al ones.

Preliminary studies were done using the SiO_2 support as catalyst (without any metal), confirming the absence of reaction even at the highest temperature tested in this work (723 K). As the most expected influence of copper nanoparticles is in the dehydrogenation step, Figure 8 summarizes the main results in

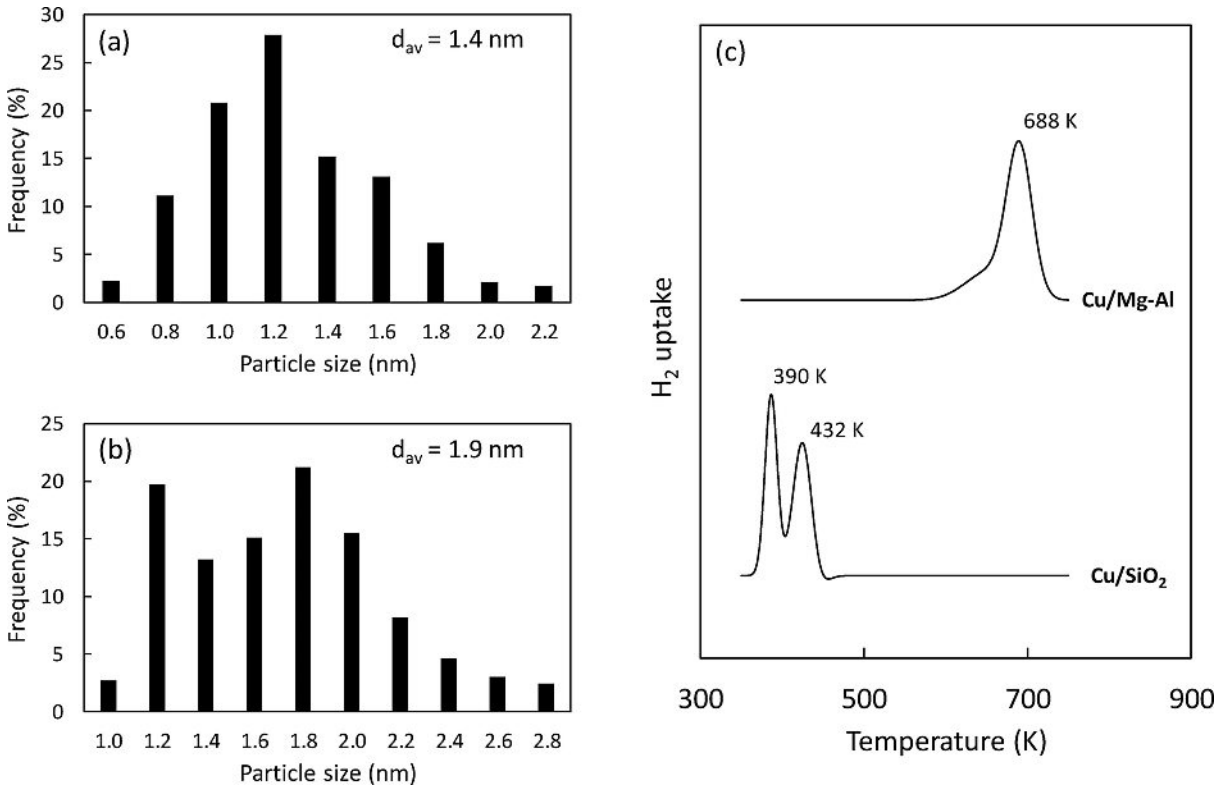

Figure 7. Particle size distribution determined by HRTEM: (a) Cu/Mg–Al, and (b) Cu/SiO_2. (c) TPR results for the Cu/Mg–Al, and Cu/SiO_2.

terms of conversion, carbon balance as well as the acetaldehyde yield. In parallel to the previous analyses, reactions were carried out under reducing and inert atmosphere. Two trends are identified when conversion is analyzed, both under inert and reducing conditions: (i) at mild conditions, temperature has the typical positive effect, increasing conversion at increasing temperatures (from 46.3% at 523 K to 77.1% at 573 K under inert conditions; and from 41.3% to 70.3% under reducing atmosphere, at similar conditions); (ii) this trend is broken at high temperatures, with a clear decreasing tendency (reaching values around 40% at 723 K), for both atmospheres. This fact suggests an undesired phenomenon that partially deactivates the material at these more severe conditions. One of the possible reasons of this behavior is the copper nanoparticle sintering (major drawback of copper regarding other metals[23]).

In order to determine the role of sintering, catalyst samples were recovered after reactions at the highest temperatures tested (723 K) while working under inert atmosphere (the most favorable conditions for crystallite agglomeration). Analyses by HRTEM showed that the copper clusters supported on the silica sintered, evolving from 1.9 to 4.1 nm of mean size. However, this phenomenon was not observed for the spent Cu/Mg–Al catalyst, keeping the size of the copper particles in the same value (HRTEM representative micrographs and particle size histograms of spent Cu/Mg–Al and Cu/SiO_2 are included in Figure S2 and S3). This fact suggests that the interaction between the support and the metal nanoparticles is stronger with Mg–Al support than with SiO_2.[12] Indeed, TPR results (Figure 7c) confirm this idea, since the reduction temperature when using Mg–Al as support is much higher than with SiO_2. (688 K with Mg–Al, and in the range of 390–430 K with SiO_2). These values are in agreement with those previously reported when using a similar mixed oxide (Zr–Al) and SiO_2.[24,25] Furthermore, the particle size histogram of the fresh Cu/SiO_2 shows a bimodal distribution that is supported by the TPR results (Figure 7b and c) since two distinguishable peaks, related to two types of clusters different in size (CuO precursors), appear within the temperature reduction range. This fact favors the particle growth: catalysts with more

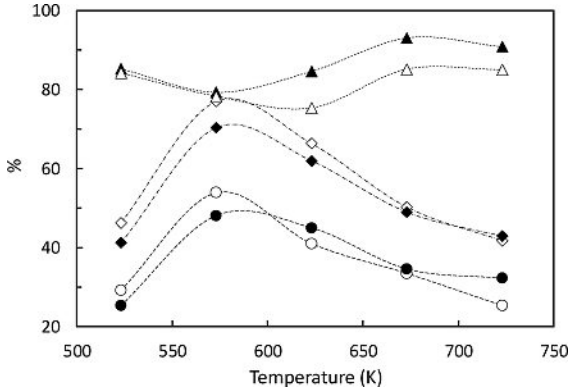

Figure 8. Conversion (◆), carbon balance closure (▲), and acetaldehyde yield (●) evolution in the ethanol gas phase condensation on Cu/SiO_2 (0.15 g). Black symbols: reducing conditions (20 NmL min^{-1} of 10 vol% H_2/He); white symbols: inert conditions (20 NmL h^{-1} of He).

heterogeneous crystallite size distribution are more prone to sintering.[26] Anyway, the increase of the copper cluster mean diameter is not too significant, since they are kept within low size (< 10 nm). Therefore, the sintering observed for the Cu/SiO_2 seems to be not the only deactivation cause.

Under reducing atmosphere, the maximum conversion matches with the minimum carbon balance (79.3 %) (Figure 8), which suggests that adsorption processes affect catalyst performance. C4 molecules (crotonaldehyde, crotyl alcohol, butanal, 1-butanol, and ethyl acetate) are identified during the reaction, being the ethyl acetate (yield up to 0.5 % at 573 K working under inert conditions) the main one. The activity of copper nanoparticles for aldolization and esterification reactions was previously observed,[2] justifying this appearance despite the catalyst has not acid/basic sites. In addition to the C4 compounds, methane and carbon monoxide were detected, indicating that acetaldehyde decarbonylation (maximum selectivity to methane of 3.4 % at 723 K under inert conditions) is taking place. Decarbonylation reaction is less relevant in the presence of copper nanoparticles regarding other metals (such as iridium, ruthenium, and platinum),[27] but the extent of this reaction is directly related to the acetaldehyde concentration. Carbon monoxide is stoichiometrically formed at the same extent as methane, but the amount observed is only around 85 % of the methane one, suggesting a strong adsorption on the metallic phase, implying its partial deactivation.[28] As a consequence, the ethanol conversion continuously decreases as temperature increases when the bimolecular and decarbonylation reactions become more important. Nevertheless, although the acetaldehyde yield decreases with the temperature (from 53.9 % at 573 K to 25.3 % at 723 K under inert conditions; and from 48.1 % to 32.2 % under reducing atmosphere, at similar conditions), its relative weight in the global amount of detected products (those shown in Scheme 1) is always higher than 95.4 and 94.6 % (723 K) in presence and absence of hydrogen, respectively. These values correspond to selectivities of 60.7 and 75.1 %, respectively. Furthermore, the water gas shift reaction could be taking place, allowing the formation of carbon dioxide due to the water presence in the reaction medium (produced from the aldol condensation step, and dehydration side-reactions).

The whole analysis of all these data requires the study of the evolution of species adsorbed on the catalytic surfaces. DRIFT spectra when working with the Cu/SiO_2 material is shown in Figure 9. Bands at wavenumbers of: 1050, 1220, 2880, 2940, and 2970 cm^{-1} related to the vibrations modes: CO stretching, C–O stretching, and CH_3 and CH_2 stretching arise at all the tested temperatures.[17] These bands are associated with the ethanol adsorption. Furthermore, a band at 1380 cm^{-1} (C–H bending vibration mode) related to acetaldehyde is observed at the lowest temperatures.[17] This last band almost disappears at the highest temperature because of the decrease of the acetaldehyde formation and the exothermic nature of the adsorption phenomenon. Because of this, the intensity of some of the adsorption bands mentioned above decreases. However, when the spectra collected under reducing and inert conditions are compared (Figure 9a and b, respectively), relevant differences at temperatures above 623 K can be noticed: (i) a band at 1740 cm^{-1} (C=O stretching vibration mode) associated with higher aldehydes (≥ C4) arises under inert conditions;[17] (ii) the band related to CH_3 and CH_2 stretching vibration modes begins growing, suggesting the formation and adsorption of higher species (≥ C4) under inert conditions. These two differences are directly related to the hydrogen feeding; when hydrogen is supplied these species formed under inert conditions are more easily reduced and desorbed. Furthermore, the presence of hydrogen also inhibits the decarbonylation of acetaldehyde (methane selectivity of 2.4 and 3.4 % at 723 K under reducing and inert conditions, respectively). Consequently, the conversions are very similar above 623 K, under reducing or inert conditions (i.e., 41.7 and 42.9 % at 723 K under inert and reducing conditions, respectively). This is not observed for the acetaldehyde yield, comparing with the two lowest temperatures at which the ethanol dehydrogenation prevails over all the reactions. Anyway, the role of the hydrogen feeding on the performance of the inverse dehydrogenation (acetaldehyde hydrogenation to ethanol) is very low since conversions are

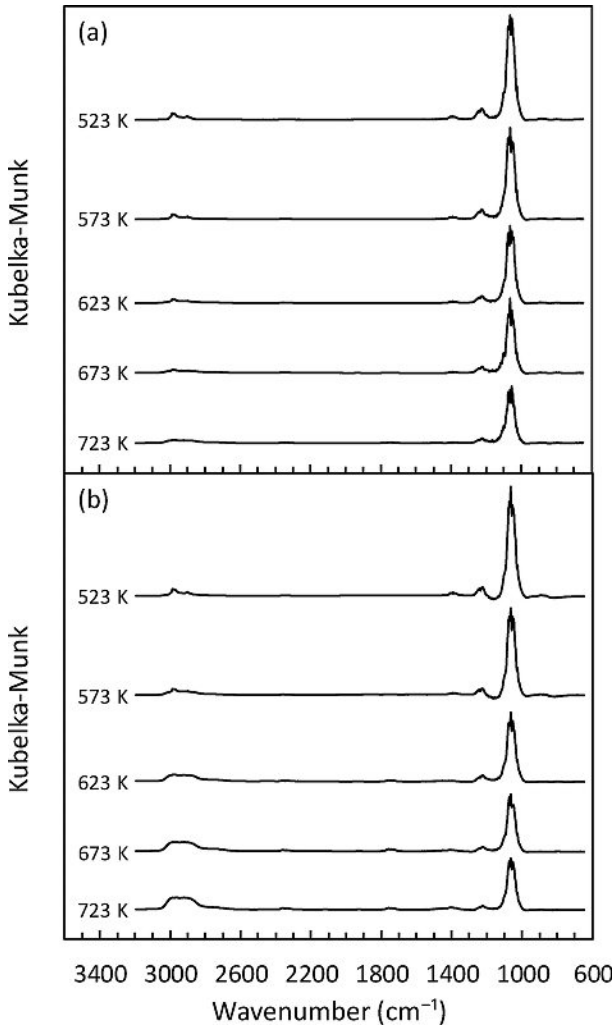

Figure 9. DRIFT spectra in the ethanol gas-phase condensation on Cu/SiO_2 under (a) reducing and (b) inert conditions.

very similar at the lowest temperatures (main difference observed at 573 K: conversion 6.8% higher working under inert conditions). Moreover, as temperature increases, the reaction extent approaches the ethanol-acetaldehyde equilibrium. Thus, at 573 K, the reaction quotient (Q), calculated with the experimental data, is around the 70 and 85% of the theoretical equilibrium constant (K) in presence and absence of hydrogen, respectively. Nevertheless, the highest approaches to ethanol-acetaldehyde equilibrium (Q/K) when working with the Cu/Mg–Al are 3 and 14% under inert and reducing conditions reached at the lowest temperature tested. In this light, copper nanoparticles are considered as a co-catalyst which favors the dehydrogenation of ethanol and the activation of the hydrogen molecule, and therefore the main step (aldolization) is only attributed to the acid-basic material (Mg–Al surface in the Cu/Mg–Al catalyst, and Mg–Al component in the physical mixture). This conclusion supports the good analysis of the physical mixture, only considering the Mg–Al component in the 1-butanol productivity calculations.

DRIFT spectra evolution with the temperature when using the Cu/Mg–Al are shown in Figure 10. In addition to the above mentioned bands, two new bands can be distinguished at 1660 and 3030 cm^{-1}, corresponding to C=C (related to crotonaldehyde and crotyl alcohol) and C–H stretching modes (associated with aldehydes).[17] The significance of the bands linked to higher unsaturated species (1660, 1740, and the band around 3000 cm^{-1}, related to C=C, C=O, and CH_3, CH_2 and CH stretching vibrations modes) is lower regarding to the previous results reported when using Mg–Al.[17] This is consistent with the lower concentration of acid sites on the Cu/Mg-Al (Table 1) being those sites that favor the stabilization of the intermediate species on the catalytic surface. There are almost no differences between the spectra at each temperature when reducing and inert conditions are compared (Figure 10a and b), with only slight differences in the intensity of the band related to the CO stretching vibration mode (1050 cm^{-1}).

As a summary of all these studies, results for the 1-butanol productivity, conversion, carbon balance closure, and selectivities to the main compounds obtained under inert conditions are different from that observed when working in presence of hydrogen. Nevertheless, concerning the physical mixture, all these evolutions are almost the same as those obtained under reducing atmosphere, as it was expected. In view of this and the DRIFT spectra, it is as if in the case of the bifunctional catalyst the hydrogen presence raised the turnover frequency of the active sites, but the species formed on the catalytic surface were the same as those generated under inert atmosphere (the degree of the surface saturation by the formed species is similar).

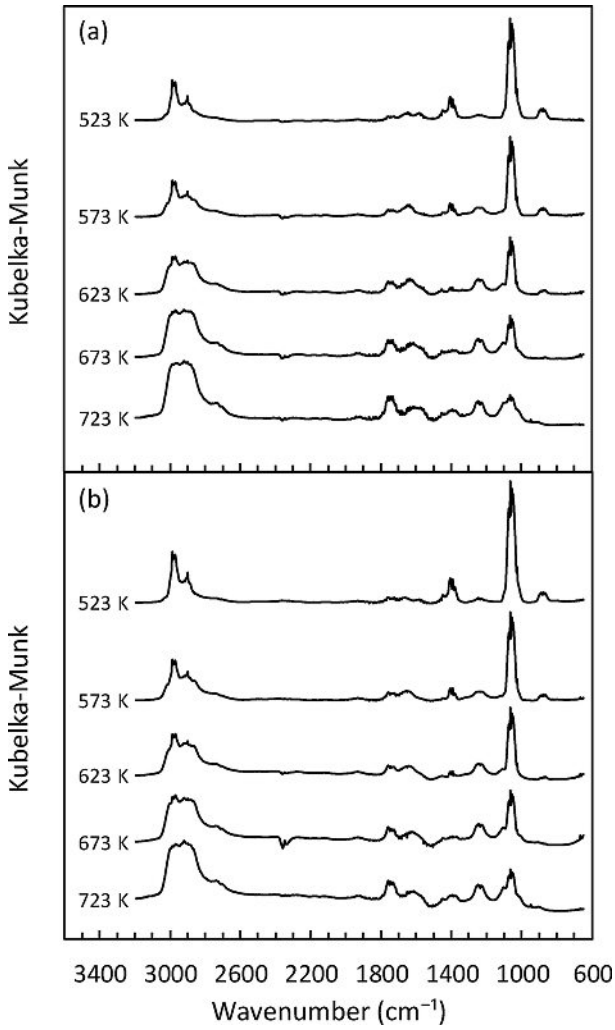

Figure 10. DRIFT spectra in the ethanol gas-phase condensation on Cu/Mg-Al under (a) reducing and (b) inert conditions.

Conclusions

The production of 1-butanol in the ethanol gas phase condensation over Mg-Al mixed oxide is enhanced by supporting copper nanoparticles, the improvement being especially significant at mild temperatures (523 and 573 K). Thus, this procedure is a very promising way to produce 1-butanol at softer conditions than the normally required. A relevant improvement in the 1-butanol productivity is achieved with only 1 wt.% of copper loading on the Mg–Al material regarding to the bare Mg–Al (12 times higher with the Cu/Mg–Al regarding to the bare Mg–Al at 523 K). This enhancement is due to the dehydrogenation ability of copper, which promotes the first step of the ethanol Guerbet reaction (acetaldehyde formation). Furthermore, when hydrogen is supplied to the reaction medium, the 1-butanol productivity improvement is even higher than under inert conditions when working with the Cu/Mg–Al catalyst because of the activation of the hydrogen molecule by copper (enhancement of 150% comparing inert and reducing conditions at 523 K). A good distribution and vicinity of the active sites involved in the different steps (mainly metal active and acid-basic sites) is considered as the key reason for the 1-butanol productivity enhancement. This conclusion is drawn by: (i) comparing in reaction under both reducing and inert conditions the bifunctional material (Cu/Mg–Al) with a physical mixture (Cu/SiO_2 + MgAl); (ii) observing

the acid-base properties that are very similar to favor the key aldolization step (similar acid-base pairs distribution and concentration between Cu/Mg–Al and Mg–Al). DRIFT spectroscopy shows that the species formed during the reaction are the same regardless of the material used (Mg–Al or Cu/Mg–Al) and the conditions (reducing or inert), suggesting that the improvement in the 1-butanol productivity is only related to an increase of the turnover frequency of the different active sites.

Experimental Section

Materials Synthesis

Mg–Al mixed oxide (Mg/Al = 3) was synthesized following the procedure detailed in a previous work.[16] The 1 wt.% Cu/Mg–Al catalyst was prepared by incipient wetness impregnation of copper (II) nitrate hydrate (Panreac) on the Mg–Al mixed oxide used as support. The resulting material was dried in an oven at 383 K for 24 h. Hereafter, it was treated in flowing air from room temperature (ca. 293 K) to 973 K with a step of 5 K min^{-1}, holding 5 hours the final temperature. Then, the Cu was reduced treating the calcined material under a mixture of 10 vol.% H_2/Ar (20 NmL min^{-1}) from room temperature (ca. 293 K) to 673 K, holding this temperature for 3 h. The reduction temperature was selected according to the results obtained during the characterization of the calcined precursor. The 1 wt.% Cu/SiO_2 catalyst was prepared under the same procedure followed as in the Cu/Mg-Al preparation using inert silica (fumed SiO_2, Aldrich) as support. Furthermore, a mechanical mixture of Cu/SiO_2:Mg–Al (1:1) was prepared by milling and pelletizing the same amounts of Cu/SiO_2 and Mg–Al mixed oxide.

Catalyst Characterization

Temperature-programmed reduction (TPR) experiments were performed in a Micromeritics AutoChem II 2920 followed by a Pfeiffer Vacuum Omnistar Prisma mass spectrometer, in order to determine the catalysts precursors reduction-temperature. The calcined materials (20 mg) were exposed under 10 vol.% H_2/Ar flow (20 NmL min^{-1}) from room temperature (ca. 293 K) to 973 K with temperature rate of 5 K min^{-1}. The textural properties of the reduced catalysts were analyzed by N_2 physisorption at 77 K, using a Micromeritics ASAP 2020 to measure the surface area, pore volume and diameter. Surface basicity and acidity were determined by temperature programmed desorption (TPD) with a Micromeritics 2900 TPD/TPR equipment. Samples of both materials (20 mg) were pretreated under flowing He (20 NmL min^{-1}) at 393 K, and saturated with CO_2 (5 NmL min^{-1}) or NH_3 (20 NmL min^{-1} of 2.5 vol% NH_3/He mixture) during 15 min. to analyze the basicity or acidity, respectively. The CO_2 and NH_3 signals evolution were monitored by mass spectrometry (Pfeiffer Vacuum Omnistar Prisma) while increasing the temperature from 298 to 973 K with a temperature ramp of 2.5 K min^{-1}. High-resolution transmission electron microscopy (HRTEM) analyses of samples of both materials were performed to determine the particle size distribution (counting a number of particles, n, higher than one hundred), using a JEOL JEM-2100 equipment. The mean particle size (d_{av}) is calculated by the following formula: $d_{av} = \sum_i n_i d_i^3 / \sum_i n_i d_i^2$, where d is the size of a specific particle.[29]

Catalytic Activity Studies

Experiments were carried out between 523 and 723 K spacing 50 K in a 0.4 cm i.d. U-shaped fixed-bed quartz reactor placed in an electric furnace PID controlled. The catalyst sample was held by a quartz wool plug, as well as the temperature was measured with a thermocouple placed close to the catalyst bed. Samples of 0.15 g of Cu/SiO_2 or Cu/Mg–Al, and 0.3 g of the physical mixture (sieved in the range 250–355 μm) were used in each experiment. These conditions were optimized in a previous paper, discarding any mass transference limitation.[17] Samples were pretreated at 523 K for 1 h under flow of 10 vol.% H_2/He mixture (20 NmL min^{-1}) previous all experiments. Absolute ethanol (≥ 99.9 %, VWR) was fed to the reactor (1.5 mL h^{-1}) injected by a syringe pump in the 10 vol.% H_2/He or He flow (20 NmL min^{-1}) depending on if the experiment is carried out under reducing or inert conditions. The resulting stream contains a 32 mol % of ethanol, being the weight hourly space velocity (WHSV) 8 h^{-1}.

The reactor outgoing effluent was on-line analyzed by gas chromatography, using a flame ionization detector (GC-FID, HP 6890Plus chromatograph). A capillary column (TRB 5MS; 30 m, 0.25 mm) was used as stationary phase. In addition, off-line GC-FID analyses (Agilent 6890N) were carried out, working with two different columns (HP-Plot Q, 30 m, 0.53 mm; and HP-Plot MoleSieve 5A, 30 m, 0.53 mm) in order to separate methane (product of acetaldehyde decarbonylation) and ethylene (from ethanol dehydration). These two light hydrocarbons cannot be separated with the GC column installed in the on-line experimental setup. The identification of the different chemical species was carried out using commercial standards in a gas chromatograph equipped with a mass spectrometer detector, GC-MS, (Shimadzu QP-2010) following the same methodology and using a similar column than in the determination of the reaction outlet gases (GC-FID).

Conversions were calculated from the ethanol concentrations at the reactor inlet and outlet streams. Carbon balances were determined checking the total quantity of carbon atoms at the reactor inlet and outlet, only considering the identified compounds (ethanol, acetaldehyde, crotonaldehyde, crotyl alcohol, 1-butanol, ethyl acetate, butanal, ethylene, diethyl ether, methane, and carbon monoxide).

The productivity of each component (i) in the reaction (or average formation rate) were calculated using Eq. (1):

$$\text{productivity of i } [\text{mmol} \cdot \text{ks}^{-1} \cdot \text{g}^{-1}] = \frac{F \cdot x \cdot \varphi_i}{W} \quad (1)$$

where F is the molar flow of ethanol supplied to the reactor in mmol ks^{-1}, *W* is the mass of catalyst in g, *x* is the ethanol conversion and φ_i is the selectivity for the formation of compound *i* in carbon basis (mol of C of ethanol converted to the component I divided by mol of C of converted ethanol).

The yield of every product was determined using Eq. (2):

$$\text{yield}_i\ [\%] = \left(\frac{\text{mol of C of ethanol converted to product i}}{\text{mol of C of ethanol fed}}\right) \cdot 100 \quad (2)$$

Infrared Spectra at Reaction Conditions

Infrared spectra were acquired by DRIFT spectroscopy with a Thermo Nicolet Nexus FT-IR equipped with a MCT/A detector. The sample of catalyst (20 mg) in each experiment was placed inside the catalytic chamber that allowed control the temperature. The

material was pretreated at 523 K for 1 hour in 10 vol.% H_2/He flow before the test. Spectra were recorded in the 650–4000 cm^{-1} wavenumber range, subtracting the KBr standard background. All signals were converted using the Kubelka-Munk method, obtaining semi-quantitative results that allow comparison between the obtained spectra. Spectra were acquired at all the reaction temperatures tested for the reactor experiments, making possible the comparison of the evolution of the compounds in the gas phase as well as on the catalytic surface.

Acknowledgements

Authors thank financial support for this work from the Ministry of Economy and Competitiveness of Spain (CTQ2014-52956-C3-1-R; CTQ2017-89443-C3-2-R). Jorge Quesada acknowledges the local Government of the Principality of Asturias for his PhD fellowship of the Severo Ochoa Program (PA-14-PF-BP14-105).

Conflict of Interest

The authors declare no conflict of interest.

Keywords: aldol reaction · C–C coupling · hydrogenation · Guerbert reaction · 1-butanol

[1] C. Angelici, B. M. Weckhuysen, P. C. A. Bruijnincx, *ChemSusChem* **2013**, *6*, 1595–1614.
[2] M. E. Sad, M. Neurock, E. Iglesia, *J. Am. Chem. Soc.* **2011**, *133*, 20384–20398.
[3] S. Wang, E. Iglesia, *J. Phys. Chem. C* **2016**, *120*, 21589–21616.
[4] S. Wang, K. Goulas, E. Iglesia, *J. Catal.* **2016**, *340*, 302–320.
[5] a) J. Sun, Y. Wang, *ACS Catal.* **2014**, *4*, 1078–1090; b) L. Faba, E. Díaz, S. Ordóñez, *Renew. Sustain. Energy Rev.* **2015**, 51, 273–287.
[6] a) H. Aitchison, R. L. Wingad, D. F. Wass, *ACS Catal.* **2016**, *6*, 7125–7132; b) S. Hanspal, Z. D. Young, H. Shou, R. J. Davis, *ACS Catal.* **2015**, *5*, 1737–1746.
[7] J. T. Kozlowski, R. J. Davis, *ACS Catal.* **2013**, *3*, 1588–1600.
[8] T. Moteki, D. W. Flaherty, *ACS Catal.* **2016**, *6*, 4170–4183.
[9] a) S. Abelló, F. Medina, D. Tichit, J. Pérez-Ramírez, J. C. Groen, J. E. Sueiras, P. Salagre, Y. Cesteros, *Chem.-Eur. J.* **2015**, *11*, 728–739; b) M. J. Climent, A. Corma, V. Fornés, R. Guil-López, S. Iborra, *Adv. Synth. Catal.* **2002**, *344*, 1090–1096; c) J. I. Di Cosimo, V. K. Díez, C. R. Apesteguía, *Appl. Catal. A Gen.* **1996**, *137*, 149–166; d) G. Zhang, H. Hattori, K. Tanabe, *Appl. Catal.* **1988**, *36*, 189–197.
[10] W. Dai, L. Ren in *Handbook of Heterogeneous Catalysis*, 2nd ed., Editors: G. Ertl, H. Knözinger, F. Schüth, J. Weitkamp, Wiley-VCH, Weinheim, **2008**, Vol. 7, pp. 3259–3262.
[11] a) A. G. Sato, D. P. Volanti, I. C. de Freitas, E. Longo, J. M. C. Bueno, *Catal. Comm.* **2012**, *26*, 122–126; b) I. C. Freitas, S. Damyanova, D. C. Oliveira, C. M. P. Marques, J. M. C. Bueno, *J. Mol. Catal. A Chem.* **2014**, *381*, 26–37.
[12] J. H. Earley, R. A. Bourne, M. J. Watson, M. Poliakoff, *Green Chem.* **2015**, *17*, 3018–3025.
[13] D. Jiang, X. Wu, J. Mao, J. Ni, X. Li, *Chem. Comm.* **2016**, *52*, 13749–13752.
[14] a) X. Wu, G. Fang, Z. Liang, W. Leng, K. Xu, D. Jiang, J. Ni, X. Li, *Catal. Comm.* **2017**, *100*, 15–18; b) J. Pang, M. Zheng, L. He, L. Li, X. Pan, A. Wang, X. Wang, T. Zhang, *J. Catal.* **2016**, *344*, 184–193.
[15] J. I. Di Cosimo, C. R. Apesteguía, M. J. L. Ginés, E. Iglesia, *J. Catal.* **2000**, *190*, 261–275.
[16] M. León, E. Díaz, S. Ordóñez, *Catal. Today* **2011**, *164*, 436–442.
[17] J. Quesada, L. Faba, E. Díaz, S. Ordóñez, *Appl. Catal. A Gen.* **2017**, *542*, 271–281.
[18] a) J. I. Di Cosimo, V. K. Díez, M. Xu, E. Iglesia, C. R. Apesteguía, *J. Catal.* **1998**, *178*, 499–510; b) S. Ogo, A. Onda, K. Yanagisawa, *Appl. Catal. A Gen.* **2011**, *402*, 188–195; c) J. T. Kozlowski, R. J. Davis, *J. Energy Chem.* **2013**, *22*, 58–64; d) L. Silvester, J. F. Lamonier, J. Faye, M. Capron, R. N. Vannier, C. Lamonier, J. L. Dubois, J. L. Couturier, C. Calais, F. Dumeignil, *Catal. Sci. Technol.* **2015**, *5*, 2994–3006; e) A. S. Ndou, N. Plint, N. J. Coville, *Appl. Catal. A Gen.* **2003**, *251*, 337–345; f) C. Yang, Z. Meng, *J. Catal.* **1993**, *142*, 37–44.; g) P. E. Hathaway, M. E. Davis, *J. Catal.* **1989**, *119*, 497–507.
[19] G. C. Bond in *Metal-Catalysed Reactions of Hydrocarbons*, Fundamental and Applied Catalysis Series, Editors: M. V. Twigg, M. S. Spencer, Springer, New York, **2005**; pp. 133–135.
[20] J. J. Ramos, V. K. Díez, C. A. Ferretti, P. A. Torresi, C. R. Apesteguía, J. I. Di Cosimo, *Catal. Today* **2011**, *172*, 141–147.
[21] D. D. Eley, M. A. Zammitt, *J. Catal.* **1971**, *21*, 366–376.
[22] M. Boudart, A. Delbouille, E. G. Derouane, V. Indovina, A. B. Walters, *J. Am. Chem. Soc.* **1972**, *94*, 6622–6630.
[23] X. Wu, G. Fang, Y. Tong, D. Jiang, Z. Liang, W. Leng, L. Liu, P. Tu, H. Wang, J. Ni, X. Li, *ChemSusChem* **2018**, *11*, 71–85.
[24] G. V. Sagar, P. V. R. Rao, C. S. Srikanth, K. V. R. Chary, *J. Phys. Chem. B* **2006**, *110*, 13881–13888.
[25] C. J. G. van der Grift, A. Mulder, J. W. Geus, *Appl. Catal.* **1990**, *60*, 181–192.
[26] G. Prieto, J. Zečević, H. Friedrich, K. P. de Jong, P. E. de Jongh, *Nat. Mater.* **2012**, *12*, 34–39.
[27] E. I. Gürbüz, D. D. Hibbits, E. Iglesia, *J. Am. Chem. Soc.* **2015**, *137*, 11984–11995.
[28] T. Bligaard, J. K. Nørskov, S. Dahl, J. Matthiesen, C. H. Christensen, J. Sehested, *J. Catal.* **2004**, *224*, 206–217.
[29] H. Arnold, F. Döbert, J. Gaube in *Handbook of Heterogeneous Catalysis*, 2nd ed., Editors: G. Ertl, H. Knözinger, F. Schüth, J. Weitkamp, Wiley-VCH, Weinheim, **2008**; Vol. 2, p. 740.

Manuscript received: March 27, 2018
Accepted Article published: June 15, 2018
Version of record online: July 10, 2018